This is the accepted manuscript made available via CHORUS. The article has been published as:

Direct Measurement of Inverse Piezoelectric Effects in Thin Films Using Laser Doppler Vibrometry

Megha Acharya, Djamila Lou, Abel Fernandez, Jieun Kim, Zishen Tian, and Lane W. Martin

Phys. Rev. Applied **20**, 014017 — Published 11 July 2023

DOI: 10.1103/PhysRevApplied.20.014017

Direct Measurement of Inverse Piezoelectric Effects in Thin Films using Laser Doppler Vibrometry

Megha Acharya,[1,2] *Djamila Lou,*[1] *Abel Fernandez,*[1] *Jieun Kim,*[1] *Zishen Tian,*[1,2] *Lane W. Martin*[1,2*]

[1] Department of Materials Science and Engineering, University of California, Berkeley, Berkeley, CA 94720, United States

[2] Materials Sciences Division, Lawrence Berkeley National Laboratory, Berkeley, CA 94720, United States

E-mail: lwmartin@berkeley.edu

Abstract

Further miniaturization of electronic devices necessitates the introduction of new materials including piezoelectric thin films exhibiting electromechanical functionalities without significant degradation in response due to substrate-induced clamping. To identify material systems with superior piezoelectric properties as thin films, simplified and quantitative electromechanical characterization techniques are required. Here, single-beam, laser-Doppler vibrometry is used to detect AC electric-field-induced surface displacement in the frequency range 1-100 kHz with low error (~6% at 10 kHz) and resolution of 0.0003 nm. The technique is used to quantify both electrostriction and piezoelectric responses (surface displacement values < 0.05 nm) of various thin films. Requirements for sample geometry and device structures are established and measurement accuracy and resolution are validated against measurements from the literature via synchrotron-based diffraction measurements. A general methodology to measure and extract the piezoelectric coefficients for thin-film samples using finite-element modeling simulations is presented and applied to determine the d_{33} coefficient and visualize the response in substrate-

clamped 50-to-400-nm-thick $PbZr_{0.52}Ti_{0.48}O_3$ films, especially as compared to bulk versions in the same sample geometry.

Introduction

Piezoelectric materials can convert electrical to mechanical energy (and vice versa) making them useful for a myriad of applications including actuation, sensing, energy harvesting, accelerometers, resonators, and filters [1–4]. Furthermore, with the pursuit of miniaturized low-power and energy-efficient devices, there is an increasing need to introduce sub-one-micron-thick films of piezoelectrics into a range of devices including micro- (MEMS) and nano-electromechanical (NEMS) systems. For example, researchers have proposed low-power piezoelectric transistors wherein applying electric field to a piezoelectric element drives a metal-to-insulator transition in a piezoresistive element, thus producing on/off states [5–7] and logic-in-memory devices (*e.g.*, the magnetoelectric spin-orbit (MESO) device) which involve manipulating magnetic spins using electric field via strain-induced coupling from thin-film piezoelectrics [8–11]. As such, there is a need to both study electromechanical responses in thin films further and to discover new thin-film systems with superior electromechanical properties. The challenge in achieving such device goals, however, is that thin-film versions (< 1 μm in thickness) of piezoelectrics typically exhibit diminished piezoelectric strains (ε) as compared to those in thick-film (> 1 μm), bulk-ceramic, or single-crystal versions due to, among other factors, clamping from the underlying substrate (> 0.5 mm-thick) [12–14]. Thus, there is a need for straightforward, widely applicable methodologies for accurately measuring electromechanical responses and, in turn, determining the direct (d_{ij}) and converse (d^*_{ij}) piezoelectric coefficients for thin-film materials.

Today, such electromechanical measurements for thin films are, in general, either challenging to complete (practically) or are subject to considerable measurement artifacts that can, if one is not extremely careful, yield quantitative results that are inaccurate. For example, scanning-probe-microscopy-based techniques like piezoresponse force microscopy (PFM) [15–18] can offer excellent vertical resolution (1-5 pm). But such techniques can be subject to numerous error-sources, including inhomogeneous electric fields concentrated near the tip [19,20], indirect topographic crosstalk [21], and dependence on optical and mechanical sensitivity of the cantilever [17,22,23], considering the measured PFM signal is representative of both the intrinsic piezoresponse and cantilever transfer function. In this regard, researchers are working on improved methods such as applying shape correction factors to account for the cantilever's dynamics [22], using interferometric displacement sensing to measure the PFM amplitude [15,16], using appropriate reference samples to identify instrumental phase offset [23], and more. Such approaches, however, remain in development. Other approaches to measure electromechanical response rely on non-contact, optical techniques based on the principles of laser-beam interferometry. Two of the most popular choices are double- and single-beam interferometry depending on the configuration of the beam-sample surface interaction. Double-beam-laser interferometry (DBLI) uses two probing beams, one each for the front and rear sides of the sample, to account for substrate bending (which can be significant for thick films). The result is a high-resolution electromechanical measurement (~0.5 pm), but one that requires intricately polished substrate surfaces and depositing large (> 400 μm diameter) [24] (and potentially thick) electrode layers owing to the requirement that the two beams remain "aligned" on the active area and due to the sensitivity of the measured surface displacement ($\vec{S}$) to the reflectivity of the electrode layers. This, in practice, makes the study of thin films challenging to impossible. Single-beam-laser

interferometry, as the name implies, uses a single probing beam and a laser-Doppler vibrometer (LDV) which detects the Doppler shift of the backscattered beam due to the electromechanical $\vec{S}$. While the resolution for the same can be more limited (~2 pm) as compared to DBLI, the sample preparation as well as the associated optical alignment is less cumbersome since one does not require highly reflective surfaces on an opaque substrate for aligning laser beams and can use electrodes that are much smaller in size (often < 50 μm in diameter). The major drawback of this technique, however, is its inability to account for substrate bending [25–29]. This said, there is a community of researchers studying thin-film heterostructures wherein the electromechanically active layers are just tens-to-hundreds of nanometers thick [30] and such heterostructures are expected to experience minimal (to no) substrate bending (as shown previously by comparing DBLI and LDV results for 1-μm-thick $PbZr_{0.52}Ti_{0.48}O_3$ films) [25]. Ultimately, it might be the case that researchers in this community can benefit from the use of the simpler LDV measurement for electromechanical measurements thereby providing access to a much wider set of researchers to potentially impact this field.

Here, a methodology to measure the electromechanical $\vec{S}$ (nm) and d_{ij}^{*} (pm/V) in epitaxial thin-film heterostructures in simple, capacitor-based device configurations using LDV is developed. In turn, the piezoelectric response of the active piezoelectric layers is quantified by first accounting for any electrostrictive effects from non-piezoelectric layers (*e.g.*, electrode layers) and applying finite-element modeling (FEM) to estimate d_{ij} (pC/N) for the active material layer. Additional discussion on the effect of film thickness and potential best practices for the community in reporting comparable results are also offered.

Working Principle – Measuring Electromechanical Strain using LDV

The electromechanical characterization of thin-film piezoelectrics with LDV requires applying electric fields across the piezoelectric layer in a capacitor-based structure with top and bottom electrodes and measuring the field-induced $\vec{S}$. In devices made from very thin piezoelectric films, however, electrostriction from non-piezoelectric layers (*e.g.*, electrodes) could contribute to the overall electromechanical response (see Appendix A for details) and thus should be quantified and (as appropriate) subtracted from the overall response to gauge the true material performance of the piezoelectric layer. Further, there needs to be a monochromatic and linearly polarized laser source accompanied by a sensor-unit for detecting the Doppler frequency-shift in the backscattered beam interacting with the moving electrode on the piezoelectric surface as compared to the reference beam to quantify the $\vec{S}$ [25,26]. The operating principle of the LDV used in this work (Polytec GmbH) and an illustration of the beam's interaction with a generic thin-film heterostructure on a substrate is shown schematically [Fig. 1(a)]. The basic function is achieved by the fact that for the laser beam (helium-neon, $\lambda = 633$ nm) any change in optical path length per unit time (*e.g.*, due to a moving surface of the piezoelectric) in the backscattered beam with respect to the reference beam will be manifested as a change in the modulation frequency of the vibrometer's response. Further, to detect the direction of the moving surface, an acoustic-optic modulator (Bragg cell) is included in the reference beam's path that shifts the reference beam's frequency as needed. This modulation frequency increases when the surface moves away from the vibrometer and decreases when the converse is true, thus providing a sense of directionality along with the magnitude of $\vec{S}$. Here, the LDV setup is operated in conjunction with a ferroelectric tester (Precision Multiferroic Tester, Radiant Technologies, Inc.) which not only electrically stimulates the films (*i.e.*, drives the electromechanical response) but also measures the polarization as a function of electric field simultaneously while concurrently converting the voltage-based response from the LDV to $\vec{S}$.

Furthermore, to address any potential ambient vibrational noise which can result in low signal-to-noise ratio (S/N), especially at low frequencies (≤ 1 kHz), the setup was placed on an active vibration-isolation stage (TS-140, Herzan LLC) within an acoustic enclosure (custom-built to reduce up to 55 dB of noise, Herzan LLC). Further, field- and frequency-dependent $\vec{S}$ measurements were performed to gauge the combined effect (if any) of the stage and the enclosure. The measured $\vec{S}$ values were found to be (essentially) the same in all cases, negating (or minimizing) the effect of any ambient-induced noise in the measured $\vec{S}$ [31]. While such additional infrastructure was not found to be critical in our testing, the situation in different laboratories might be different and such consideration might be necessary to confront the environmental noise levels felt locally.

Sample Geometry Considerations

Observations about sample geometry configurations form a critical part of studying any metrology technique. As such, this section provides a summary of the specific sample and device requirements to measure piezoelectric films (< 1 μm thick) with low $|\vec{S}|$ (< 1 nm), fabricated on semi-infinite substrates. In this regard, one of the central questions to be addressed is if the mechanical interaction of a micropositioner probe tip can impact the magnitude of measured electromechanical response of the film [31]? As a test, a piezoelectric heterostructure of the from 45 nm $SrRuO_3$ / 200 nm $PbZr_{0.52}Ti_{0.48}O_3$ / 45 nm $SrRuO_3$ / $SrTiO_3$ (001) (which were produced via pulsed-laser deposition using established processes [30–32]) was studied in two device configurations [Fig. 1(b)]: type-I devices are based on standard capacitor structures routinely used in the community to electrically investigate samples by directly contacting the capacitor surface

and type-II devices based on a specially designed offset platinum contact pad that allows for (indirect) minimal probe-tip interaction with the capacitor structure itself [Fig. 1(c-d)] [31,33].

In turn, the polarization and electromechanical response of the type-I and -II devices were measured as a function of applied field using a tungsten micropositioner probe tip (3.5 μm probe-tip diameter; SE-20T, Lucas/Signatone Corp.) using LDV. The film exhibited a robust ferroelectric hysteresis loop when probed electrically using either device type [Fig. 1(e)] [31]. Further, the $\vec{S}$ values for both the device types were found to be essentially the same [Fig. 1(f)]. Thus, it appears that touching the probe tip directly on the top electrode (type-I device) does not adversely affect the electromechanical response to a measurable extent. Furthermore, it is also important to note that many of the as-measured electromechanical responses were slightly asymmetric under positive and negative bias, but that the asymmetry would switch when we switched the drive and ground connections (*i.e.*, the responses were mirror images to each other). As such, our standard procedure throughout this study (and our recommended procedure) is to measure the heterostructures in a type-I-device configuration in two ways: 1) drive top electrode and ground bottom electrode and 2) drive bottom electrode and ground top electrode and then to take (and present) the average response to account for any potential measurement artifacts [31].

Establishing Measurement Reproducibility and Accuracy

Building from the work to establish baseline needs for sample geometry for piezoelectric characterization of thin films, efforts were undertaken to assess the reproducibility and accuracy of the measurements. To establish one measure of reproducibility, the location of the laser spot was changed relative to a fixed probe tip in a 100-μm-diameter type-I device [Fig. 2(a)]. Regardless of the laser position (five different locations on the same contact were tested) and

different intensities of contacting the tip, the $\vec{S}$ values were essentially unaffected. This suggests that the measurement is robust against measurement-to-measurement (user-to-user) variability in setting up the study, in part owing to the simplicity of the measurement approach. In turn, we proceeded to evaluate the accuracy of LDV-based measurements. For the desired assessment, the values for electric field-induced ε were obtained as a function of applied field at 10 kHz [Fig. 2(b)] for 400 nm-thick $PbZr_{0.52}Ti_{0.48}O_3$ films (produced via the same process noted before [31]) using LDV and compared that to the results obtained using synchrotron-based measurements for 400 nm-thick $PbZr_{0.45}Ti_{0.55}O_3$ films from the literature [34,35]. Synchrotron-based *in operando* X-ray microdiffraction studies provide precise, real-time measurements of changes in lattice parameters with applied electric field. While this approach can be highly accurate in providing information on a film's electromechanical response, it should be emphasized that it often requires type-II devices (or similarly complex devices) and one to have ready access to a high brightness X-ray source (like a synchrotron) as in the work of Refs. [33,36]. Our choice of test material was motivated, in part, by the fact that this material has been studied extensively over the years, including by such synchrotron-based approaches and in similar geometries. Thus, this provides a wonderful reference to explore how this laboratory-based methodology compares.

In making this comparison, however, it should be noted that there can be contributions from electrostriction due to the electrode layers in LDV measurements (something that does not happen for the synchrotron-based studies where the strain is extracted from shifts in diffraction peaks arising solely from the $PbZr_{0.45}Ti_{0.55}O_3$ layer). To probe this idea, the ε arising from electrostriction from a 100 nm $SrRuO_3$ / $SrTiO_3$ (001) heterostructure in the same device geometry was measured using LDV [Fig. 2(c)] and, subsequently, subtracted from the overall LDV-based strain. Assuming the resistivity for the 100 nm $SrRuO_3$ / $SrTiO_3$ (001) heterostructure is 250 μΩ-

cm [37], the electric field across the $SrRuO_3$ layer when used as an electrode in the $SrRuO_3$/ $PbZr_{0.52}Ti_{0.48}O_3$/$SrRuO_3$ heterostructure is expected to be lower than 1 kV/cm which accounts for a $\varepsilon < 0.015\%$. As a result, even with the correction, the LDV-based ε is comparable in magnitude with that for the synchrotron-based studies [Fig. 2(b)]; thus, validating the accuracy of LDV-based measurements. Furthermore, it is worth noting that the $\vec{S}$ values measured for the $SrRuO_3$ electrode are electrostrictive in nature and hence, as low as 0.025 nm in magnitude at 35 kV/cm; consistent with the instrument's resolution specifications of 0.0003 nm (Polytec GmbH). Building on this study of small electrostrictive responses, we further probed the electromechanical response of a non-piezoelectric dielectric [38] in the form of a 35 nm $La_{0.7}Sr_{0.3}MnO_3$/65 nm $BaZrO_3$/35 nm $La_{0.7}Sr_{0.3}MnO_3$/$(LaAlO_3)_{0.3}(Sr_2TaAlO_6)_{0.7}$ (001) heterostructure [Fig. 2(d)] across which an electric field as high as 1000 kV/cm could be applied and where electrostrictive effects of magnitude similar to that for $SrRuO_3$ were observed in the $La_{0.7}Sr_{0.3}MnO_3$-based electrodes. The heterostructure exhibited $|\vec{S}|$ as low as 0.008 nm after subtracting the electrostrictive contributions from the electrodes ($La_{0.7}Sr_{0.3}MnO_3$) from the overall response; effectively allowing us to probe the resolution limits of the instrument even further. From these studies, it appears that LDV can be considered as an accurate and high-resolution technique for the quantification of piezoelectric and electrostrictive responses in thin films without requiring complex, fabrication-intensive device configurations.

Procedures to Minimize Error

We completed additional studies to probe pathways to limit measurement noise and error, including a series of frequency-dependent studies which are reported here. At lower frequencies ($\leq$ 1 kHz), LDV measurements are known to exhibit a low S/N which can be increased by

improving the signal amplitude ($|\vec{S}|$), using a relatively thicker film [39]. To confirm this, both 200-nm- (*i.e.*, the same reported in Figure 1) and 400-nm-thick $PbZr_{0.52}Ti_{0.48}O_3$ films (*i.e.*, the same reported in Figure 2) were driven up to a field of 250 kV/cm (to facilitate ferroelectric polarization switching) at 1, 10, and 100 kHz (preferred frequency range for low-loss electrical response [32]). As expected, the 400-nm-thick films were found to possess higher $|\vec{S}|$ (and hence, higher S/N) [31]. For brevity, we thus focus on further frequency-dependent studies on the 400-nm-thick films [Fig. 3(a)-(c)]. Even for a 400-nm-thick film [wherein the measured $|\vec{S}|$ is small (< 1 nm)], the measurements are expected to be influenced by acoustic noise (generated by ambient mechanical noise and vibrations in the lab) for frequencies ≤ 1 kHz. Similarly, there is a higher probability of signal distortion for frequencies ≥ 100 kHz as the signal frequency approaches the limits of the sensor unit. Thus, by default, one might expect that measurements in the intermediate frequency range (*i.e.*, around ~10 kHz) would offer the best opportunity for reducing such signatures of noise and signal distortion. This is, in fact, confirmed by the frequency-dependent ε measurements which present average errors of 34%, 6%, and 12% for measurements at 1, 10, and 100 kHz, respectively [Fig. 3(d)-(f)] [31]. Analyzing the data further, the converse d_{ij}^* in pm/V ($= d\varepsilon/dE$ where E is the applied field) was extracted from the measurements at 1, 10, and 100 kHz and found to be in the range of 41-54 pm/V; values consistent with the synchrotron-based measurements (*i.e.*, 42-53 pm/V [34]). Ultimately, while for the current study of thin films (< 400 nm in thickness) the best S/N was obtained at 10 kHz, the same might not necessarily be true for any given sample geometry or material system. Thus, the recommended procedure would be to determine the error percentages at an applied field large enough to enable ferroelectric switching while varying the frequency across a reasonably wide range of frequencies (*e.g.*, 0.1-100 kHz) to identify the frequency regime with the lowest S/N for the sample under consideration.

Assessing Direct Piezoelectric Coefficients using Finite-Element Modeling

Having established a protocol for measuring $\vec{S}$ and obtaining the converse d_{ij}^{*} coefficients for these thin-film heterostructures using LDV, we proceed to estimate the direct d_{ij} coefficients using the measured $|\vec{S}|$ and finite-element modeling (FEM)-based simulations. The process that is used is visualized in a workflow. In brief, the $|\vec{S}|$ resulting from the piezoelectric layer is obtained after subtracting the contribution due to electrode-induced electrostriction [Fig. 4(a)]. Then a cylindrical model representing the piezoelectric layer is built (see Appendix B for details) that simulates the appropriate mechanical (*i.e.,* clamping due to substrate along the bottom and the surrounding film along the curved surface) and electrical (*i.e.*, bias on the unclamped top surface) constraints to not only estimate d_{ij} but also its evolution across the layer's thickness [Fig. 4(b)].

As a demonstration of the workflow, 50-, 100-, 200-, and 400-nm-thick $PbZr_{0.52}Ti_{0.48}O_3$ films (produced using the same process noted above [31]) were measured using LDV and analyzed via FEM [Fig. 5(a-b)]. $|\vec{S}|$ was measured and simulated at a field of 250 kV/cm, considering the simulations were performed at a constant bias and not as a function of frequency, the LDV-based $|\vec{S}|$ values used were measured at 10 kHz, where measurement-related error percentages are minimal [Fig. 5(c)]. The FEM simulations allow one to explore the cross-sectional (or through-thickness) evolution of the piezoelectric layers which indicates different $|\vec{S}|$ (and hence d_{ij}) values at the piezoelectric-bottom electrode ($|\vec{S}|^{min}$and d_{33}^{min}) and top electrode-piezoelectric film ($|\vec{S}|^{max}$and d_{33}^{max}) interfaces for all heterostructure thicknesses (with 50- and 400-nm-thick films shown as an example) studied herein [Fig. 5(d-e)]. Focusing on d_{33}, akin to $|\vec{S}|$, the values were found to increase linearly from d_{33}^{min} (≈ 0 due to clamping from the semi-infinite, semi-rigid substrates) to d_{33}^{max} with increasing distance from the substrate. While d_{33}^{max} provides a measure

of the ultimate response of the material, it might also be responsible to use d_{33}^{avg} (= (d_{33}^{min}+d_{33}^{max})/2) if one were to report a single value of response for the film (both are listed here, Fig. 5(c)]. Such a gradient in $|\vec{S}|$ and d_{33} [Fig. 5(d-e)], however, is expected to be dependent on the mechanical constraints imposed on the piezoelectric layer. As an example, if the constraints due to the surrounding film along the curved surface can be removed by simulating the effect of lateral scaling through 4-μm-sized islands clamped on a substrate instead of a continuous film, $|\vec{S}|^{max}$ and d_{33}^{max} are expected to be enhanced significantly, both experimentally and in FEM simulations.

Apart from the gradient in values along a particular cross-section, across different heterostructures, the $|\vec{S}|$ increases (albeit not simply in a linear fashion) with film thickness and both the d_{33}^{max} and d_{33}^{avg} vary highly non-linearly, with little change in both for films from 50 to 200 nm, but significant increases for films that are 400 nm thick. Furthermore, as expected, the measured $|\vec{S}|$ (and corresponding d_{33}^{avg}) was the lowest (highest) for the 50- (400-) nm-thick $PbZr_{0.52}Ti_{0.48}O_3$ films owing to a relatively high (reduced) effect of clamping. Additionally, it is interesting to note that the d_{33}^{avg} for the 100- and 200-nm-thick films were not only equal in value, but also just 3.5% higher than that for the 50-nm-thick films, making this measurement valuable in detecting even minor changes in material properties. Concurrently, the d_{33}^{avg} for the 400-nm-thick films was 20% higher than that for the 50- to 200-nm-thick films. Further, we can compare the efficiency of electrical-to-mechanical energy conversion for the $PbZr_{0.52}Ti_{0.48}O_3$ thin films to bulk versions using the electromechanical coupling coefficient, $k_{33}^2 = \frac{d_{33}^2}{\epsilon_0 \epsilon_r s_{ij}}$ where ϵ_0 is the permittivity of free space, ϵ_r is the relative permittivity (dielectric constant), and s_{ij} is the elastic compliance. As a reference, we use the values reported for bulk $PbZr_{0.52}Ti_{0.48}O_3$ ceramics with ϵ_r = 1250 and d_{33}= 223 pC/N [40]. Assuming the elastic compliance (s_{ij}) is the same for the thin-

film and the bulk versions, the appraisal of the $PbZr_{0.52}Ti_{0.48}O_3$ films was done using the ratio $\left(\frac{d_{33}^{max}}{\sqrt{\epsilon_r}}\right)_{film} \Big/ \left(\frac{d_{33}^{max}}{\sqrt{\epsilon_r}}\right)_{bulk}$, where $\left(\frac{d_{33}^{max}}{\sqrt{\epsilon_r}}\right)_{bulk} = 6.3$. To do this, additional DC bias-dependent dielectric studies were performed to estimate ϵ_r for each film thickness and the values varied from 654 (50 nm) to 746 (400 nm) with a minimum of 470 for the 200-nm-thick films [31]. While, in general, one might expect ϵ_r to increase with increasing film thickness, owing to the decreasing effect of substrate-induced clamping, the enhancement in ϵ_r at lower thicknesses can be attributed to the presence of in-plane polarized *a* domains in addition to out-of-plane polarized *c* domains [41,42]. For the sake of brevity, we do not dive deeper into the trend in thickness-dependent dielectric response in the $PbZr_{0.52}Ti_{0.48}O_3$ films. Instead, circling back to the electromechanical studies, comparing the fraction of k_{33} for the different films reveals that, when normalized to the dielectric response there is relatively little difference between the films in this thickness regime. While are films give values between 50-63% of bulk performance suggesting that they are all of similar quality and that (at least in this thickness range) the effect of clamping on the response is rather substantial (as might be expected) [Fig. 5(c)] [31]. This said, the combined LDV and FEM approach provides a robust way to characterize and understand the electromechanical response of thin films and could be a highly beneficial technique for future studies in this spirit.

Summary

We demonstrate what we hope is a feasible and relatively straightforward methodology for measuring electric field-induced $|\vec{S}|$ in < 1 μm thick films using LDV while exploring numerous intricacies in terms of sample geometry, accuracy, resolution, and procedural limitations. First, the

effect of sample geometry was probed, establishing that standard, out-of-plane capacitor structures are likely adequate for measuring the electromechanical responses in thin films without the need for specialized device configurations. Further, the measurement accuracy was tested by comparing the ε obtained using LDV for 400 nm-thick $PbZr_{0.52}Ti_{0.48}O_3$ films to that using synchrotron-based measurements while establishing the need to account for electrostriction-induced ε due to the electrodes in a probed heterostructure. Owing to an instrument-provided resolution of 0.0003 nm, $|\vec{S}|$ in non-piezoelectric electrodes and dielectric layers were successfully measured with values as low as 0.0025 nm and 0.0008 nm, respectively. Additionally, field- and frequency-dependent studies were performed on 400 nm-thick $PbZr_{0.52}Ti_{0.48}O_3$ films to assess the operational limits of the measurement in the 1-100 kHz range using appropriate error evaluation (the lowest error of 6% was found at 10 kHz). The experimental studies were augmented by FEM simulations which were applied to a thickness series of 50-400-nm-thick $PbZr_{0.52}Ti_{0.48}O_3$ films, to extract value of d_{33}^{max} and d_{33}^{avg} and enabling comparison with bulk versions via the use of the electromechanical coupling coefficient. In conclusion, we provide a comprehensive methodology for quantitative electromechanical characterization of thin films using LDV and FEM which hopefully lessens the barrier to entry for those working in thin films to study electromechanical responses.

Acknowledgments

This work was primarily supported by the U.S. Department of Energy, Office of Science, Office of Basic Energy Sciences, Materials Sciences and Engineering Division under Contract No. DE-AC02-05-CH11231 (Materials Project program KC23MP) for the discovery of novel functional materials. D.L. acknowledges the support of the Army Research Office under Grant W911NF-21-1-0118 and the Air Force. A.F. acknowledges support from the Army Research Office under Grant

No. W911NF-21-1-0118. J.K. acknowledges the support of the Army Research Office under Grant No. W911NF-21-1-0126. Z.T. acknowledges the support of the National Science Foundation under Grant DMR-2102895. L.W.M. acknowledges additional support from the Army Research Laboratory as part of the Collaborative for Hierarchical Agile and Responsive Materials (CHARM) under cooperative agreement W911NF-19-2-0119.

Appendix A: Description of Electromechanical Response in Thin-Film Heterostructures

The overall electromechanical response (ε) of a material is the result of both electrostriction and piezoelectricity. Electrostriction, which is present in all materials, is a change in shape in response to electric field that is proportional to the square of the applied field, does not depend on the direction of the applied field, and is (generally) considerably smaller than the piezoelectric effect. It arises from the anharmonicity of ion-pair potential such that when a field is applied, the ions rearrange their relative position and move apart [43,44]. Piezoelectricity, on the other hand, occurs only for a sub-set of materials with non-centrosymmetric crystal structures and the resulting ε is directly proportional to the applied field (via the *converse* effect). While it also arises from ionic anharmonicity, the latter additionally exhibits charge separation in response to mechanical forces (via the *direct* effect) [45,46]. Though both effects have been utilized in applications, piezoelectricity often results in a higher electromechanical coupling.

Appendix B: Finite-Element Modeling of Piezoelectric Response in Thin-Film Heterostructures

The device simulations have been performed using FEM in the simulation software *COMSOL Multiphysics* (https://www.comsol.com/). Therein, simulating any physical phenomenon, such as piezoelectricity, involves finding solutions to partial differential equations (PDE) which can be simulated for a generic geometrical domain by parsing it into multiple, finite-sized and interconnected elements. The associated equations are applied to each of the elements to provide approximate solutions for the entire domain. The accuracy and the computing time for the simulation are affected by the elemental size and distribution. In the current study, the primary modules required are *solid mechanics* and *electrostatics* which can be used as a combination in

the *MEMS* (microelectromechanical system) physics interface designed specifically for the devices in the micron-scale dimensions to generate both direct and converse piezoelectric effect.

Constitutive equations for piezoelectric effects: The PDE demonstrating electromechanical coupling between mechanical displacement (u) and electric potential (φ) in a piezoelectric film with a mass density ϱ, is as shown:

$$-\varrho\ddot{u} + \nabla.[s^{-1}.\nabla u] + \nabla.[d.s^{-1}.\nabla\varphi] + f = 0 \qquad \text{(A1)}$$

$[s]$ and $[d]$ represent the elastic compliance and the (direct) piezoelectric coefficient matrix, respectively. Further, the mechanical stress ($\vec{T}$) and electric field ($\vec{E}$) can be related to the mechanical forces (f) and φ as $\vec{T} + f = \varrho\ddot{u}$ and $\vec{E} = -\nabla\varphi$, respectively. After simplification, the equations can be expressed in a strain-charge matrix form as $\vec{S} = [s]\vec{T} + [d^t]\vec{E}$ where $\vec{S}$ (which depends on the numerical solutions for u) represents the mechanical surface displacement and $[d^t]$ is the transpose of $[d]$. As noted above, the solutions for the governing PDE are obtained for each of the parsed elements in the piezoelectric domain and combined to represent overall $|\vec{S}|$ response of the geometry.

Defining sample geometry and composition: While the MEMS interface can simulate a myriad of device architectures, we focus on a simple geometrical configuration herein. Here, the capacitor heterostructure has been visualized as a piezoelectric layer with composition $PbZr_{0.52}Ti_{0.48}O_3$ in a cylinder 4 µm in diameter (emulating the laser spot dimensions) and 50-400 nm in height. It is important to note that in the real-world scenario, the piezoelectric layers are stacked between two electrode layers, however, in modeling the simulations we can skip the electrode layers as their function (of applying an electrical bias across the piezoelectric layer in the heterostructure) is being accounted for by defining appropriate electrical boundary conditions for the same layer. Further, as elucidated in the main text; the goal of this study is determining the

piezoelectric coefficients of a thin-film heterostructure. The piezoelectric response in thin films is primarily affected by two material parameters: $[s]$ and $[d]$. Considering the elements for $[s]$ are challenging to be estimated for $PbZr_{0.52}Ti_{0.48}O_3$ as thin films, we assume the values to be the same as that for bulk $PbZr_{0.52}Ti_{0.48}O_3$ ceramics as shown:

$$s^{E}_{ij} = \begin{bmatrix} 13.8 & -4.07 & -5.8 & 0 & 0 & 0 \\ -4.07 & 13.8 & -5.8 & 0 & 0 & 0 \\ -5.8 & -5.8 & 17.1 & 0 & 0 & 0 \\ 0 & 0 & 0 & 48.2 & 0 & 0 \\ 0 & 0 & 0 & 0 & 48.2 & 0 \\ 0 & 0 & 0 & 0 & 0 & 38.4 \end{bmatrix} \qquad \text{(A2)}$$

values in ×10^{-12} 1/Pa

To estimate the elements for $[d]$, we start with the d_{31} and d_{33} values for bulk $PbZr_{0.52}Ti_{0.48}O_3$ ceramics (*i.e.*, 93.5 and 223 pC/N) [40] as the first iteration of the simulation, as shown:

$$d_{ij} = \begin{bmatrix} 0 & 0 & 0 & 0 & 494 \\ 0 & 0 & 0 & 494 & 0 \\ -93.5 & -93.5 & 223 & 0 & 0 \end{bmatrix}$$

values in ×10^{-12} C/N

Considering, the piezoelectric coefficients for ceramics are much higher in magnitude as compared that in films, d_{31} and d_{33} values have been decreased systematically until the simulated $|\vec{S}|$ matches with that of the experimentally obtained values. After, multiple iterations, the value for d_{31} was kept fixed at -50 pC/N for all the simulated $PbZr_{0.52}Ti_{0.48}O_3$ piezoelectric layers, while the d_{33} values varied from 82.1 to 102.5 pC/N with increasing the thickness of the layer from 50 to 400 nm to obtain simulated $|\vec{S}|$ close to that of the experimental $|\vec{S}|$ which ranged from 0.025 to 0.445 nm. It is important to note that we focus on the more relevant coefficients (d_{31} and d_{33}) and are unable to estimate the d_{15} values (associated with a transverse device configuration) with the current longitudinal device configuration (*i.e.,* where the direction of electric field is parallel to that of the $|\vec{S}|$).

Defining parameters for Physics I (Solid Mechanics): Using the solid mechanics part of the module, clamping due to the substrate and the surrounding film on the active volume of the capacitor heterostructure has been introduced by applying a fixed mechanical constraint to the bottom and the curved surface of the cylinder-shaped piezoelectric domains, respectively. Apart from the geometry of the domain, the imposed mechanical constraints are expected to affect $\vec{T}$ and hence, the simulated $|\vec{S}|$.

Defining parameters for Physics II (Electrostatics): Using the electrostatics part of the module, an electric field (250 kV/cm) across the thickness of the heterostructure has been emulated by applying an electric potential (1.25, 2.5, 5, and 10 V) to the top and ground (0 V) to the bottom surface of the cylinder with height 50, 100, 200, and 400 nm, respectively. Such electrical boundary conditions are expected to affect $\vec{E}$ and hence, the simulated $|\vec{S}|$.

Defining meshing parameters: As mentioned earlier, defining elemental size and distribution in the mesh can be critical for accuracy and compute-time. Here, a user-controlled mesh with the elemental size calibrated for 'General Physics' with the minimum element size as small as 0.8 nm has been used. Further, considering the three-dimensional cylinder geometries with a high aspect ratio are challenging to be modelled due to limited possibilities for an efficient elemental distribution, the swept meshing technique has been used which involves mapping the elemental distribution on the top surface of the cylinder on to the curved and the bottom surface, generating an efficient and accurate finite element mesh.

References

[1] Y. Q. Fu, J. K. Luo, N. T. Nguyen, A. J. Walton, A. J. Flewitt, X. T. Zu, Y. Li, G. McHale, A. Matthews, E. Iborra *et al.*, *Advances in Piezoelectric Thin Films for Acoustic Biosensors, Acoustofluidics and Lab-on-Chip Applications*, Prog Mater Sci **89**, 31 (2017).
[2] S.-G. Kim, S. Priya, and I. Kanno, *Piezoelectric MEMS for Energy Harvesting*, MRS Bull **37**, 1039 (2012).
[3] C. B. Eom and S. Trolier-McKinstry, *Thin-Film Piezoelectric MEMS*, MRS Bull **37**, 1007 (2012).
[4] Y. Yoshino, *Piezoelectric Thin Films and Their Applications for Electronics*, J Appl Phys **105**, 061623 (2009).
[5] R. Keech, S. Shetty, M. A. Kuroda, X. H. Liu, G. J. Martyna, D. M. Newns, and S. Trolier-McKinstry, *Lateral Scaling of* $Pb(Mg_{1/3}Nb_{2/3})O_3$*-*$PbTiO_3$ *Thin Films for Piezoelectric Logic Applications*, J Appl Phys **115**, 234106 (2014).
[6] M. Copel, M. A. Kuroda, M. S. Gordon, X.-H. Liu, S. S. Mahajan, G. J. Martyna, N. Moumen, C. Armstrong, S. M. Rossnagel, T. M. Shaw *et al.*, *Giant Piezoresistive On/Off Ratios in Rare-Earth Chalcogenide Thin Films Enabling Nanomechanical Switching*, Nano Lett **13**, 4650 (2013).
[7] D. M. Newns, B. G. Elmegreen, X. Liu, and G. J. Martyna, *High Response Piezoelectric and Piezoresistive Materials for Fast, Low Voltage Switching: Simulation and Theory of Transduction Physics at the Nanometer‐ Scale*, Adv. Mater. **24**, 3672 (2012).
[8] J. Irwin, S. Lindemann, W. Maeng, J. J. Wang, V. Vaithyanathan, J. M. Hu, L. Q. Chen, D. G. Schlom, C. B. Eom, and M. S. Rzchowski, *Magnetoelectric Coupling by Piezoelectric Tensor Design*, Sci Rep-Uk **9**, 19158 (2019).
[9] W. Zhao, J. Kim, X. Huang, L. Zhang, D. Pesquera, G. A. P. Velarde, T. Gosavi, C.-C. Lin, D. E. Nikonov, H. Li *et al.*, *Low‐ Voltage Magnetoelectric Coupling in* $Fe_{0.5}Rh_{0.5}/0.68PbMg_{1/3}Nb_{2/3}O_3$*‐ 0.32*$PbTiO_3$ *Thin‐ Film Heterostructures*, Adv. Funct. Mater. **31**, 2105068 (2021).
[10] S. Manipatruni, D. E. Nikonov, and I. A. Young, *Beyond CMOS Computing with Spin and Polarization*, Nat Phys **14**, 338 (2018).
[11] S. Manipatruni, D. E. Nikonov, C.-C. Lin, T. A. Gosavi, H. Liu, B. Prasad, Y.-L. Huang, E. Bonturim, R. Ramesh, and I. A. Young, *Scalable Energy-Efficient Magnetoelectric Spin–Orbit Logic*, Nature **565**, 35 (2019).
[12] J. L. Zhao, H. X. Lu, J. R. Sun, and B. G. Shen, *Thickness Dependence of Piezoelectric Property of Ultrathin* $BiFeO_3$ *Films*, Phys B Condens Matter **407**, 2258 (2012).
[13] R. N. Torah, S. P. Beeby, and N. M. White, *Experimental Investigation into the Effect of Substrate Clamping on the Piezoelectric Behaviour of Thick-Film PZT Elements*, J Phys D Appl Phys **37**, 1074 (2004).
[14] V. Nagarajan, A. Roytburd, A. Stanishevsky, S. Prasertchoung, T. Zhao, L. Chen, J. Melngailis, O. Auciello, and R. Ramesh, *Dynamics of Ferroelastic Domains in Ferroelectric Thin Films*, Nat Mater **2**, 43 (2003).
[15] L. Collins, Y. Liu, O. S. Ovchinnikova, and R. Proksch, *Quantitative Electromechanical Atomic Force Microscopy*, ACS Nano **13**, 8055 (2019).
[16] A. Labuda and R. Proksch, *Quantitative Measurements of Electromechanical Response with a Combined Optical Beam and Interferometric Atomic Force Microscope*, Appl Phys Lett **106**, 253103 (2015).

[17] R. Proksch, *In-Situ Piezoresponse Force Microscopy Cantilever Mode Shape Profiling*, J Appl Phys **118**, 072011 (2015).
[18] S. Lepadatu, M. Stewart, and M. G. Cain, *Quantification of Electromechanical Coupling Measured with Piezoresponse Force Microscopy*, J Appl Phys **116**, 066806 (2014).
[19] T. Jungk, Á. Hoffmann, and E. Soergel, *Influence of the Inhomogeneous Field at the Tip on Quantitative Piezoresponse Force Microscopy*, Appl Phys **86**, 353 (2007).
[20] A. Abdollahi, N. Domingo, I. Arias, and G. Catalan, *Converse Flexoelectricity Yields Large Piezoresponse Force Microscopy Signals in Non-Piezoelectric Materials*, Nat Commun **10**, 1266 (2019).
[21] S. M. Yang, L. Mazet, M. B. Okatan, S. Jesse, G. Niu, T. Schroeder, S. Schamm-Chardon, C. Dubourdieu, A. P. Baddorf, and S. V. Kalinin, *Decoupling Indirect Topographic Cross-Talk in Band Excitation Piezoresponse Force Microscopy Imaging and Spectroscopy*, Appl Phys Lett **108**, 252902 (2016).
[22] N. Balke, S. Jesse, P. Yu, B. Carmichael, S. V. Kalinin, and A. Tselev, *Quantification of Surface Displacements and Electromechanical Phenomena via Dynamic Atomic Force Microscopy*, Nanotechnology **27**, 425707 (2016).
[23] S. M. Neumayer, S. Saremi, L. W. Martin, L. Collins, A. Tselev, S. Jesse, S. V. Kalinin, and N. Balke, *Piezoresponse Amplitude and Phase Quantified for Electromechanical Characterization*, J Appl Phys **128**, 171105 (2020).
[24] T. Liu, P. Tipsawat, W. Zhu, T. N. Jackson, M. Sivaramakrishnan, P. Mardilovich, T. Schmitz-Kempen, and S. Trolier-McKinstry, *Challenges in Double-Beam Laser Interferometry Measurements of Fully Released Piezoelectric Films*, J Appl Phys **131**, 214102 (2022).
[25] M. Pokorny, M. Sulc, R. Herdier, D. Remiens, E. Dogheche, and D. Jenkins, *Measurement Methods for the d_{33} Coefficient of PZT Thin Films on Silicon Substrates: A Comparison of Double-Beam Laser Interferometer (DBI) and Single-Beam Laser Vibrometer (LDV) Techniques*, Ferroelectrics **351**, 122 (2007).
[26] P. Castellini, *Laser Doppler Vibrometry, A Multimedia Guide to Its Features and Usage* (2020).
[27] S. Shetty, J. I. Yang, J. Stitt, and S. Trolier-McKinstry, *Quantitative and High Spatial Resolution d_{33} Measurement of Piezoelectric Bulk and Thin Films*, J Appl Phys **118**, 174104 (2015).
[28] A. L. Kholkin, C. Wütchrich, D. V. Taylor, and N. Setter, *Interferometric Measurements of Electric Field‐ induced Displacements in Piezoelectric Thin Films*, Rev Sci Instrum **67**, 1935 (1996).
[29] Q. M. Zhang, W. Y. Pan, and L. E. Cross, *Laser Interferometer for the Study of Piezoelectric and Electrostrictive Strains*, J Appl Phys **63**, 2492 (1988).
[30] J. Karthik, A. R. Damodaran, and L. W. Martin, *Epitaxial Ferroelectric Heterostructures Fabricated by Selective Area Epitaxy of $SrRuO_3$ Using an MgO Mask*, Adv. Mater. **24**, 1610 (2012).
[31] See Supplemental Material at [URL Will Be Inserted by Publisher] for [Effect of Vibration and Acoustic Isolation on the Electromechanical Response, Growth of Thin Film Heterostructures, Motivation for Using Device Types I and II, Microfabrication Processes for Device Type I and II, Measurement of Asymmetry in Electromechanical Response, Measurement of Electrostrictive Contribution Due to $SrRuO_3$, Measurement of Dielectric Polarization and Electromechanical Response in 65 nm-thick $BaZrO_3$ films, Measurement of Electromechanical Response in 200 nm-thick $PbZr_{0.52}Ti_{0.48}O_3$ Film as a Function of Applied Field and Frequency for Error-analysis,

Comparison of Electromechanical response in 400 nm- and 200-nm thick $PbZr_{0.52}Ti_{0.48}O_3$ films using Error-analysis, Measurement of Ferroelectric Polarization in 400 nm-thick $PbZr_{0.52}Ti_{0.48}O_3$ Films, X-ray Diffraction Studies on 50-200 nm-thick $PbZr_{0.52}Ti_{0.48}O_3$ Films, Dielectric Studies on 50-400 nm-thick $PbZr_{0.52}Ti_{0.48}O_3$ Films, Electromechanical Modeling Using COMSOL on 50-400 nm-thick $PbZr_{0.52}Ti_{0.48}O_3$ Films as a Function of Thickness.]
[32] E. Lupi, A. Ghosh, S. Saremi, S. Hsu, S. Pandya, G. Velarde, A. Fernandez, R. Ramesh, and L. W. Martin, *Large Polarization and Susceptibilities in Artificial Morphotropic Phase Boundary $PbZr_{1-x}Ti_xO_3$ Superlattices*, Adv Electron Mater **6**, 1901395 (2020).
[33] J. Kim, D. J. Meyers, A. Kumar, A. Fernandez, G. A. P. Velarde, Z. Tian, J.-W. Kim, J. M. LeBeau, P. J. Ryan, and L. W. Martin, *Frequency-Dependent Suppression of Field-Induced Polarization Rotation in Relaxor Ferroelectric Thin Films*, Matter **4**, 2367 (2021).
[34] D.-H. Do, A. Grigoriev, D. M. Kim, C.-B. Eom, P. G. Evans, And E. M. Dufresne, *In Situ X-Ray Probes for Piezoelectricity in Epitaxial Ferroelectric Capacitors*, Integr Ferroelectr **101**, 174 (2008).
[35] D.-H. Do, P. G. Evans, E. D. Isaacs, D. M. Kim, C. B. Eom, and E. M. Dufresne, *Structural Visualization of Polarization Fatigue in Epitaxial Ferroelectric Oxide Devices*, Nat Mater **3**, 365 (2004).
[36] J. Kim, A. Kumar, Y. Qi, H. Takenaka, P. J. Ryan, D. Meyers, J.-W. Kim, A. Fernandez, Z. Tian, A. M. Rappe, *et al. Coupled Polarization and Nanodomain Evolution Underpins Large Electromechanical Responses in Relaxors*, Nat Phys **18**, 1502 (2022).
[37] R. Gao, Y. Dong, H. Xu, H. Zhou, Y. Yuan, V. Gopalan, C. Gao, D. D. Fong, Z. Chen, Z. Luo *et al.*, *Interfacial Octahedral Rotation Mismatch Control of the Symmetry and Properties of $SrRuO_3$*, ACS Appl Mater Inter **8**, 14871 (2016).
[38] G. Łupina, J. Dąbrowski, P. Dudek, G. Kozłowski, P. Zaumseil, G. Lippert, O. Fursenko, J. Bauer, C. Baristiran, I. Costina *et al.*, *Dielectric Constant and Leakage of $BaZrO_3$ Films*, Appl Phys Lett **94**, 152903 (2009).
[39] P. F. O'Malley, J. F. Vignola, and J. A. Judge, *Amplitude and Frequency Dependence of the Signal-to-Noise Ratio in LDV Measurements*, Volume 1 23rd Bienn Conf Mech Vib Noise Parts B 545 (2011).
[40] D. A. Berlincourt, C. Cmolik, and H. Jaffe, *Piezoelectric Properties of Polycrystalline Lead Titanate Zirconate Compositions*, Proc Ire **48**, 220 (1960).
[41] J. C. Agar, Y. Cao, B. Naul, S. Pandya, S. V. D. Walt, A. I. Luo, J. T. Maher, N. Balke, S. Jesse, S. V. Kalinin *et al.*, *Machine Detection of Enhanced Electromechanical Energy Conversion in $PbZr_{0.2}Ti_{0.8}O_3$ Thin Films*, Adv. Mater. **30**, 1800701 (2018).
[42] J. C. Agar, R. V. K. Mangalam, A. R. Damodaran, G. Velarde, J. Karthik, M. B. Okatan, Z. H. Chen, S. Jesse, N. Balke, S. V. Kalinin *et al.*, *Tuning Susceptibility via Misfit Strain in Relaxed Morphotropic Phase Boundary $PbZr_{1-x}Ti_xO_3$ Epitaxial Thin Films*, Adv Mater Interfaces **1**, 1400098 (2014).
[43] A. A. Gundjian, *The Electrostrictor - A New Type of Electromechanical Semiconductor Oscillator*, 1965 Int Electron Devices Meet 35 (1965).
[44] C. L. Hom and N. Shankar, *A Fully Coupled Constitutive Model for Electrostrictive Ceramic Materials*, J Intel Mat Syst Str **5**, 795 (1994).
[45] M. E. Lines and A. M. Glass, *Principles and Applications of Ferroelectrics and Related Materials*, in (Oxford Classic Texts in the Physical Sciences, 2001), pp. 1–23.
[46] S. Trolier-McKinstry, *Piezoelectric and Acoustic Materials for Transducer Applications*, in edited by A. S. & E. K. Akdoğan (Springer, Boston, MA., 2008), pp. 39–56.

Figures and captions

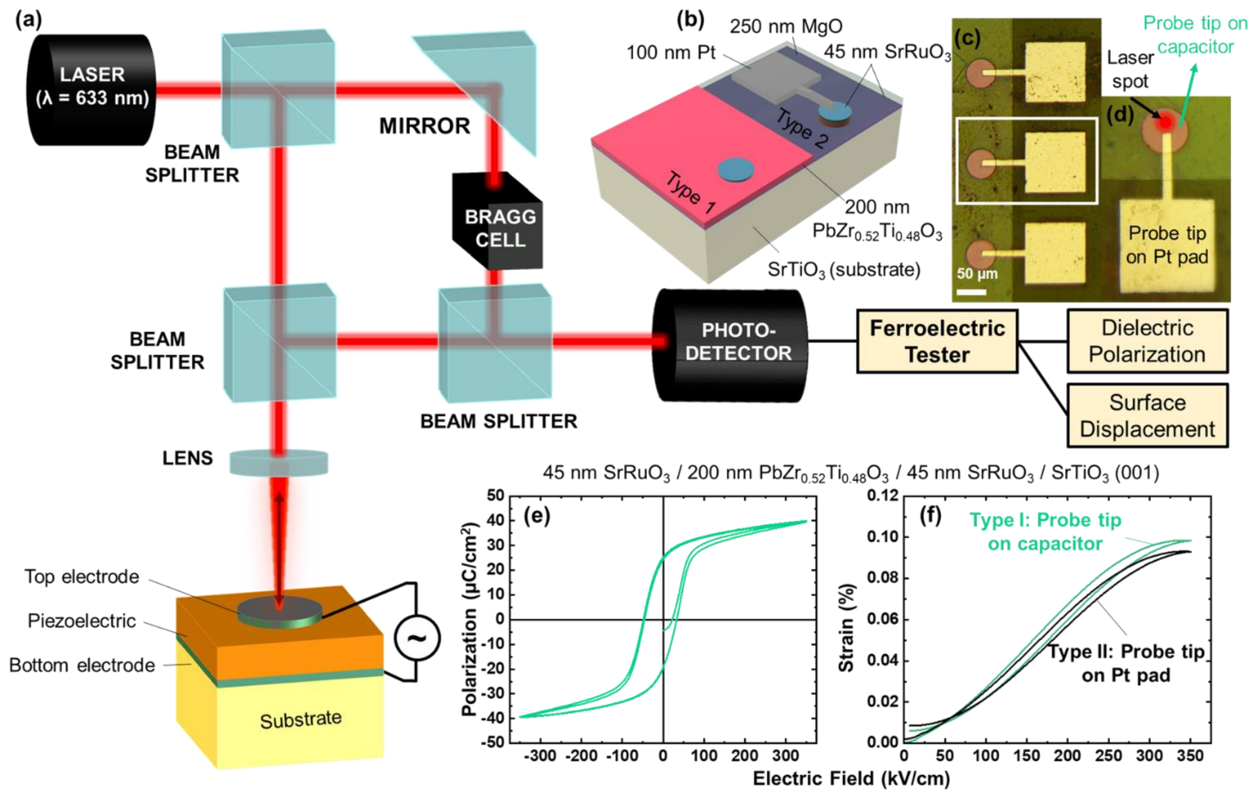

Figure 1. (a) Schematic representing the basic measurement principle in a laser Doppler vibrometer (LDV) setup and the alignment of the laser beam with respect to a generic thin-film heterostructure. (b) Schematic showing the type-I and -II device configurations. (c-d) Optical microscopy-based images of the type-II device configuration. For the same 45 nm $SrRuO_3$/400 nm $PbZr_{0.52}Ti_{0.48}O_3$/45 nm $SrRuO_3$/$SrTiO_3$ (001) heterostructure, the (e) polarization-electric field hysteresis loops and (f) strain-electric field loops both measured at a frequency of 10 kHz in both type-I and -II device configurations.

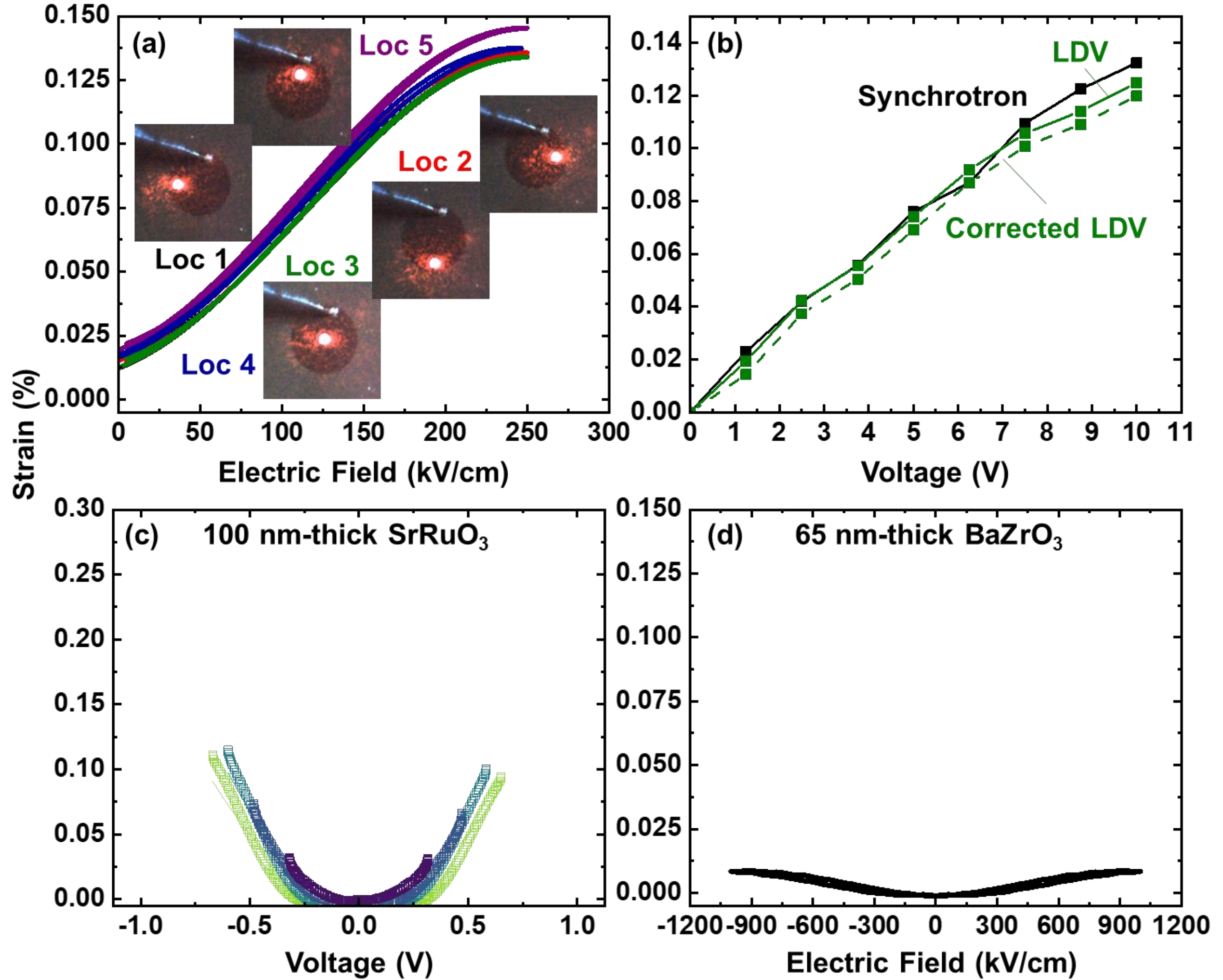

Figure 2. (a) Strain-electric field loops (under positive bias only for brevity) measured at a frequency of 10 kHz for a 45 nm $SrRuO_3$/200 nm $PbZr_{0.52}Ti_{0.48}O_3$/45 nm $SrRuO_3$/$SrTiO_3$ (001) heterostructure with the laser spot (red) focused at five different locations (Loc 1 – Loc 5) on the surface of a 100-µm-diameter type-I-device capacitor. (b) Comparison of the strain as a function of applied voltage between *in operando* synchrotron-based microdiffraction studies for a 400-nm-thick $PbZr_{0.45}Ti_{0.55}O_3$ film (adapted from Refs. 34, 35) and LDV-based measurements for a 45 nm $SrRuO_3$/400 nm $PbZr_{0.52}Ti_{0.48}O_3$/45 nm $SrRuO_3$/$SrTiO_3$ (001) heterostructure using the same device configuration as Fig. 1(d-e). (c) Strain as a function of applied voltage for a 100 nm $SrRuO_3$ / $SrTiO_3$ (001) heterostructure used to estimate the electrostriction of the electrodes. (d) Strain-electric field loops 35 nm $SrRuO_3$/65 nm $BaZrO_3$/35 nm $SrRuO_3$/$SrTiO_3$ (001) heterostructure used to demonstrate LDV's ability to measure even very small electrostrictive responses. All measurements shown here have been conducted at an applied frequency of 10 kHz.

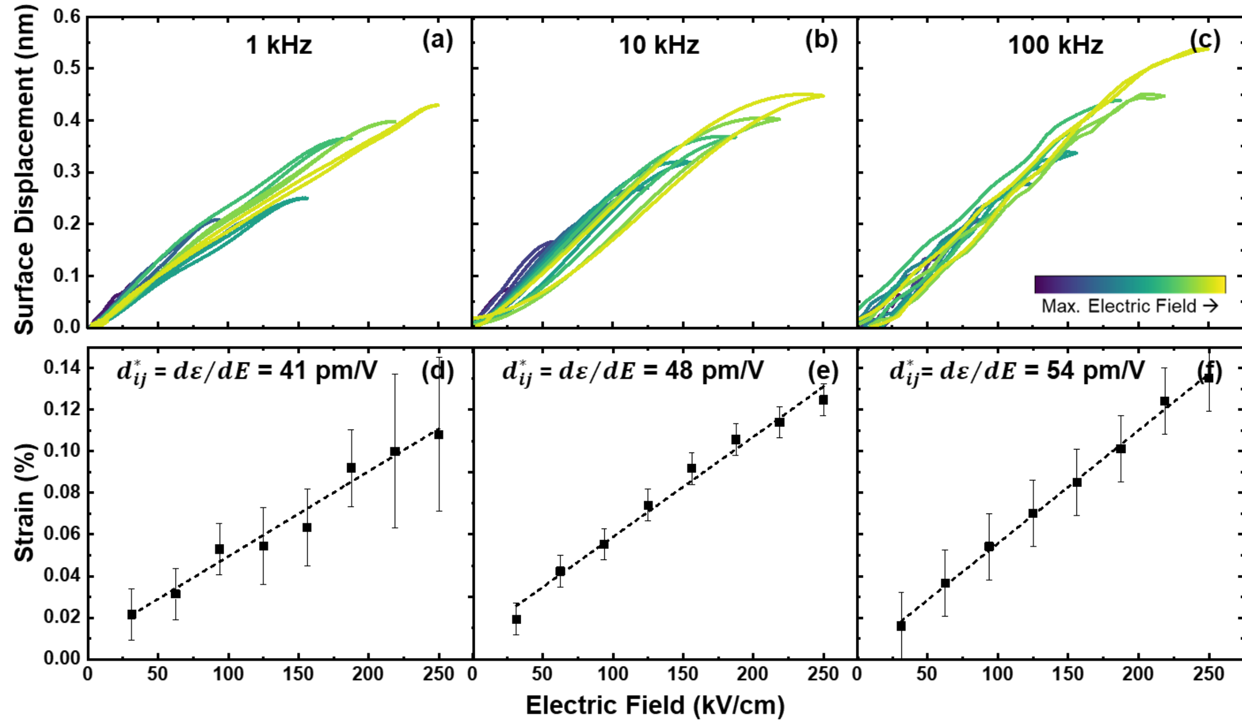

Figure 3. Surface displacement loops (top row) and strain (with associated error percentages) as a function of applied electric field (shown for positive bias only for brevity) for a 45 nm $SrRuO_3$/400 nm $PbZr_{0.52}Ti_{0.48}O_3$/45 nm $SrRuO_3$/$SrTiO_3$ (001) heterostructure at a measurement frequency of (a,d) 1 kHz, (b,e) 10 kHz, and (c,f) 100 kHz. Corresponding d_{ij}^{*} values extracted from the data are shown as well.

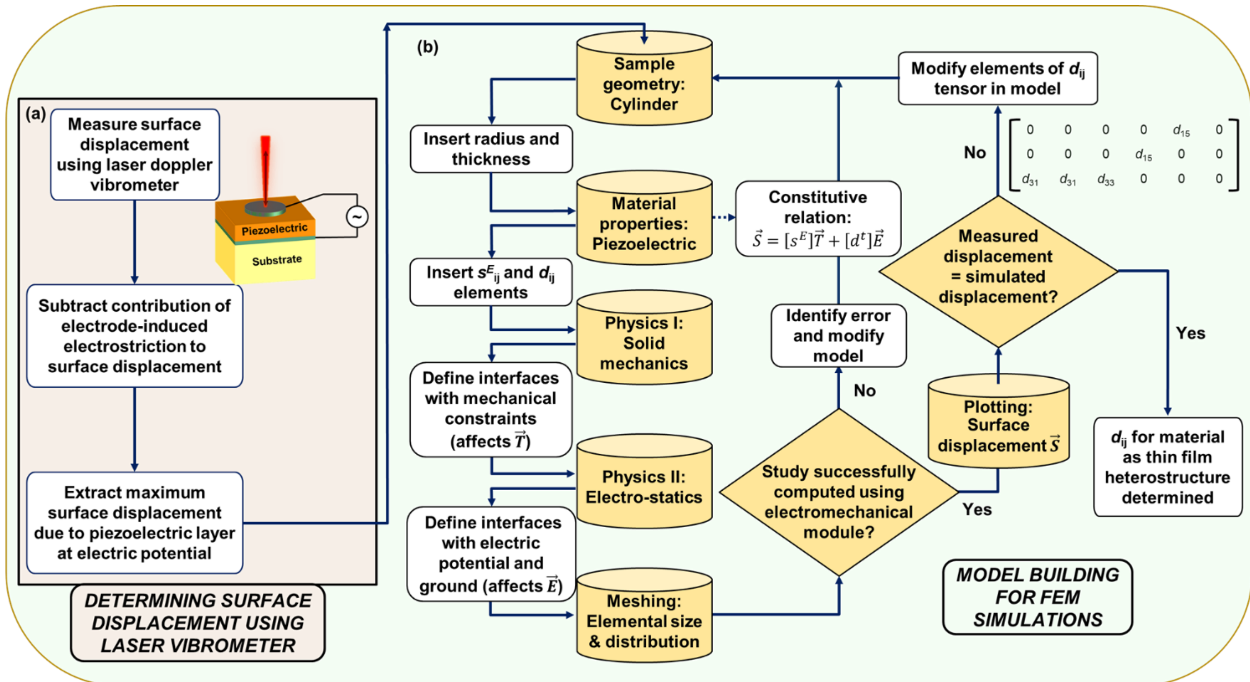

Figure 4. Proposed workflow for determining the piezoelectric coefficients (d_{31} and d_{33}) in any thin-film heterostructure, starting from (a) measuring the surface displacement using LDV due to the piezoelectric layer followed by (b) finite element modeling (FEM)-based simulations to estimate the relevant elements in the piezoelectric tensor.

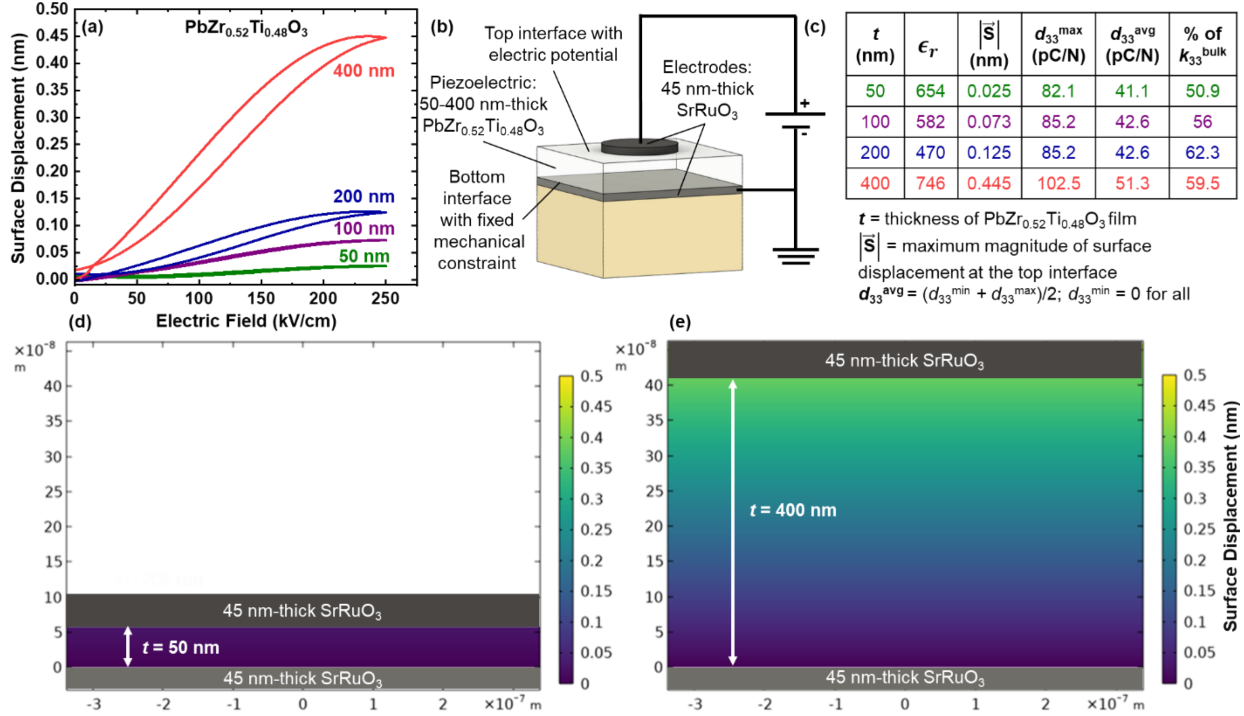

Figure 5. (a) Surface piezoelectric displacement loops as a function of electric field (positive bias) at a frequency of 10 kHz for 45 nm $SrRuO_3$/50, 100, 200, and 400 nm $PbZr_{0.52}Ti_{0.48}O_3$/45 nm $SrRuO_3$/$SrTiO_3$ (001) heterostructures. (b) Schematic showing the interfaces with an electric potential and a fixed mechanical constraint in the simulated device configuration. (c) Table providing a summary of the ϵ_r, $|\vec{S}|$, d_{33}^{avg}, and % k_{33}^{bulk} values, where d_{33}^{min} and d_{33}^{max} are obtained from the minimum and the maximum values for $|\vec{S}|$ at the bottom and the top interface, respectively. Cross-section of the (d) 50- and (e) 400-nm-thick $PbZr_{0.52}Ti_{0.48}O_3$ films with the colormap indicating the variation in $|\vec{S}|$ as a function of distance from the mechanically constrained bottom surface at an electric field of 250 kV/cm applied to the top surface, estimated using finite element modeling-based simulations.